2026 IEEE/SICE International Symposium on System Integration (SII)
January 11-14, 2026. Cancún, México

An Articulated-arm Underwater Mobile and Manipulation Robot with Thrusters for Both Suction and Propulsion "Lamprey-1"

–Calculation of Adhesive Force for Negative Pressure Effect Plate Required During Wall Suction Work and Its Verification Experiments–

Shota Hiromoto[1], Atsushi Kakogawa[1], and Norimitsu Sakagami[2]

***Abstract*— This paper proposes an articulated-arm underwater robot with a suction mechanism, which includes thrusters for both suction and propulsion. A robotic arm encounters fluid resistance during manipulation. However, generating a suction force using a propulsion thrusters enable stable manipulation. This suction force depends on the arm's movement. In this research, the suction force required to attach the wall was estimated based on a dynamic model that includes fluid resistance. The experiment revealed the relationship between the input value of the electric speed controller (ESC) for thrusters and the suction force. Furthermore, the experiment showed that the developed robot can maintain suction to a pool wall with this estimated suction force. Results confirmed that the proposed dynamic model can estimate the required suction force for 10 out of 12 arm-end trajectories.**

I. INTRODUCTION

Recently, various underwater robots have been utilized for maintenance and inspection of infrastructures such as dams, bridge piers, offshore wind power plants, oil platforms, and ship hulls [1]. Previous underwater robots primarily focused on camera-based inspections such as Remotely Operated Vehicles (ROVs), where the robot's underwater mobility was crucial. However, the need to attach manipulators and perform various tasks is also growing. For those applications, the configuration of ROVs equipped with a single arm-gripper have been typically commercialized so far. In the TRIDENT project [2] and the MARIS project [3], an experiment to grip a cylindrical object was conducted with a single manipulator. They confirmed that the gripping success rate of 70% was achieved in the pool by compensating for disturbances from tidal currents with large thruster outputs and feedback from a single camera.

On the other hand, when greater operational stability is required, anchoring the drifting robot to underwater structures have been also employed. These are primarily classified into three types: fixation via dual-arm structures, magnetic adhesion, and thruster adhesion. The first is the underwater robot with two arms which can anchor itself with one arm and execute tasks with the other [4]–[6]. However, pole-like structures such as handrails or stakes are necessary for the robot to easily anchor its entire body. The second is the method simply anchor the robot body using magnetic force [7]. It consumes less energy during anchoring compared to other methods. However, there is a limitation in environments where the target surface must be magnetic material. The third involves pressing the robot against the target surface by using the propulsion force of a thruster for locomotion [8], [9]. It does not require special structures for grasping and materials for magnetic adhesion to anchor the robot. It even allows the robot to move while pressing against the wall. However, as with ordinary suction cups in air, flatness is required on the surface to be adhered to. To date, the concept of a negative pressure effect plate (NPEP) has been proposed to maximize the adsorption force of the thruster [10], [11]. Using this method, even if the surface has slight irregularities, the adhesive force will not be significantly reduced. Therefore, this study proposes an arm-type underwater swimming-manipulation robot equipped with a base unit featuring thrusters with the NPEP for suction and movement named "Lamprey-1".

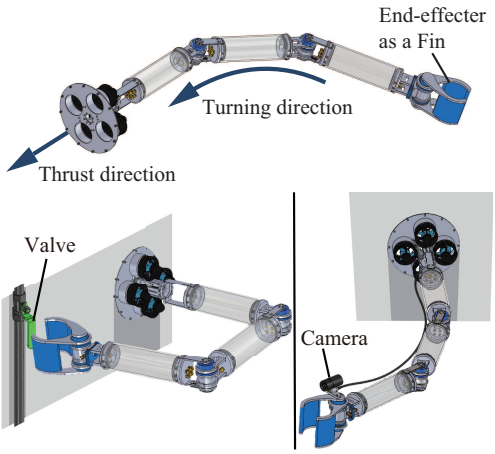

Fig. 1. Conceptual illustration of the articulated-arm underwater mobile and manipulation robot "Lamprey-1"

Figure 1 shows the conceptual illustration of Lamprey-1. Although this structure itself has already been reported in our previous research [12], the one in this study differs in that it has an increased number of arm joints and thrusters,

*This work was supported by JSPS KAKENHI Grant Number 23K22727.

[1]S. Hiromoto and A. Kakogawa are with the Department of Robotics, Faculty of Science and Engineering, Ritsumeikan University, 1-1-1 Noji-higashi, Kusatsu, Shiga 525-8577, JAPAN rr0130ie@ed.ritsumei.ac.jp, kakogawa@fc.ritsumei.ac.jp

[2]N. Sakagami is with the Department of Mechanical Engineering and Robotics, Faculty of Advanced Science and Technology, Ryukoku University, 1-5 Seta-Oecho-Yokotani, Otsu, Shiga 520-2194, JAPAN sakagami@rins.ryukoku.ac.jp

resulting in greater degrees of freedom. By varying the rotational speeds of multiple thrusters, it is possible to generate movements like pivot turns. However, it is also possible to change the swimming direction by using the hand at the arm-end like a fin. This latter method allows for a longer moment arm, enabling more efficient robot's turning motion. This configuration enables both reliable base fixation through suction (supporting arm reaction forces) and underwater swimming mobility. Therefore, this research aims to apply the robot to fields previously achievable only through labor-intensive methods using human divers, such as fixed-point camera observation in fast-flowing underwater environments, hull cleaning, and opening/closing underwater valves.

To realize a robot that could be considered the ideal form for this underwater mobility task, several technical hurdles must be overcome. For example, if Lamprey-1 is driven by battery power, reducing energy consumption during underwater operations directly translates to longer operating times. Unlike the arm joints, the thrusters must continue rotating to maintain adhesion to the wall, and this is what causes the greatest reduction in battery charge. Therefore, an operating method that avoids unnecessary thruster rotation is required. The thruster thrust force (adhesive force) required for the robot's adhesion depends on the fluid resistance experienced by the moving arm. If the arm-end moves towards the wall, scooping water outwards, it tends to peel the base away from the wall. Conversely, if the arm-end pushes water away from the wall, the thrusters can adhere to the wall with minimal adhesive force.

This paper conducted a dynamic analysis and underwater experiments using an actual device to clarify the relationship between the arm's motion patterns and the required adhesive force of the thrusters. Specifically, simulations and experiments were compared to assess the detachment potential of the negative pressure effect plate under twelve different arm-end position trajectories and velocity patterns.

II. MECHANICAL STRUCTURE AND CONTROL SYSTEM

Figure 2 shows the actual overview of Lamprey-1 which consists of a single two-joints-arm with a gripper hand and four thrusters equipped in the same direction. The total weight (in air) is 11.4 kg and its length is 1.8 m. The three links are composed of two aluminum end caps and an acrylic pipe, which are sealed with two O-rings for waterproofing. The end of Link 1 (bottom of the robot) has four thrusters (T200 Thruster; Blue Robotics Inc., CA, USA), which are utilized for propulsion and suction. The NPEP is also attached to the bottom to amplify the suction force. Twelve equally spaced natural rubber bumpers are placed on the outer circumference of the NPEP's bottom surface. These bumpers have two functions: they reduce the sliding of the suction surface and maintain a distance between the surface and the NPEP. 3D-printed tubes are placed between the thrusters and the NPEP to guide the water flow. The end

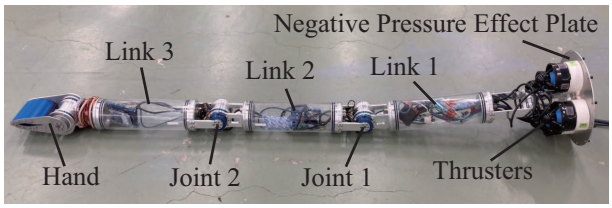

Fig. 2. Overview of the articulated-arm underwater mobile and manipulation robot "Lamprey-1"

of the Link 3 (arm-end of Lamprey-1) has a simple two-fingered gripper as an end-effector that weighs 2.23 kg in the air.

Submersible geared electric servo motors [13], [14], developed in our previous work, are used for the actuators of the two joints, and thus the aluminum casing is not waterproofed with a sealant or other materials. Therefore, it allows water to enter the inside of the actuator. The actuators are comprised of resin gears (S-Bear DD; STARLITE Inc., Osaka, Japan) and ceramic bearings, which have a low friction property in the sliding part without lubricant. As a result, rough torque measurement in underwater environment without a force/torque sensor is possible based on the motor current sensing [13]. The joint actuators are comprised of the same motors used in our previous work (RI50 KV100; CubeMars Inc., Jiangxi, China) [13], [14] that we rust-proofed by ourselves, an epoxy-resin-waterproofed Hall sensor board, and an epoxy-resin-waterproofed encoder board (AS5048A; ams OSRAM Inc., Steiermark, Austria).

Figure 3 shows the control and communication system of the robot. The ground equipment consists of a leader Arduino, a laptop for data acquisition, and a DC 24 V power supply (max. 400 W). This board transmits and receives the joint data with the followers via CAN BUS communication. Inside Link 1, electric speed controllers (ESCs) (Basic ESC; Blue Robotics Inc.) to drive the thrusters are mounted. Inside Link 2 and 3, motor drivers (ESCON Module 50/5; Maxon Group, Obwalden, Switzerland), and microcontroller (Arduino Uno R4 Minima; Arduino S.R.L., Monza, Italy) are installed.

Each link of Lamprey-1 was designed to achieve neutral buoyancy. However, at the present stage, the positions of the center of buoyancy and center of gravity have not been considered. Furthermore, since the actual unit exhibits deviations from the design values, this experiment employed weights and floats to manually align their positions. This prevents Lamprey-1 from sinking or rising in water, ensuring that the robot's center of gravity and center of buoyancy remain unchanged even during the arm movement.

III. SUCTION FORCE ESTIMATION FOR STABLE MANIPULATION

Here, the suction force of the thrusters required for wall adhesion, which varies with the armi-end trajectory, is numerically evaluated.

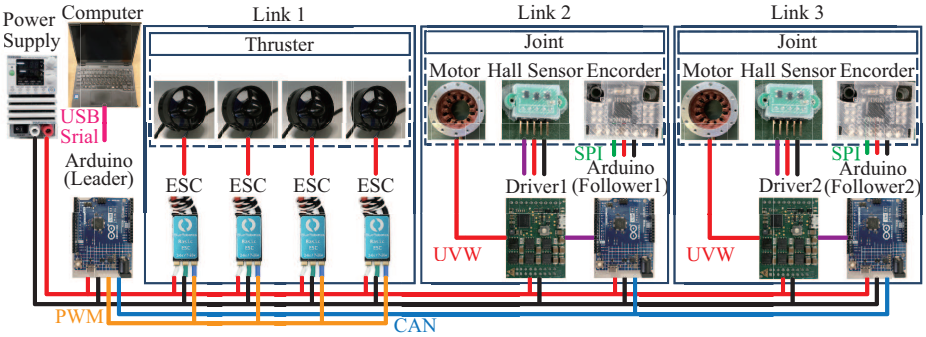

Fig. 3. Control and communication system of the robot

A. Dynamic model of the robot

Kinematic and dynamic model of the Lamprey-1 is shown in Fig. 4 (a). As in the real robot, the model comprises three links, and Link 1 is assumed to be fixed to the wall surface. Considering each link as a cylinder, the added-mass for Link 1 and 2 can be calculated by

$$m_{\mathrm{add},i} = \frac{1}{4} C_{m,i} \rho \pi D^2 l_i \tag{1}$$

where C_m, ρ [kg/m^3], D [m], and l_i [m] denote the added-mass coefficient, the fluid density, the link diameter, and i-th link length, respectively. Those added mass were added to the original mass of each link.

The fluid drag force on each link is calculated using the strip theory approach. The force on the j-th segment ($j = 1, 2, 3...$) is divided along the link's direction. The relationship between the fluid drag force on each segment and the velocity perpendicular to the links can be calculated as follows:

$$f_{d,ij} = \frac{1}{2} C_{d,i} \rho v_{ij}^2 S \tag{2}$$

where $f_{d,ij}$ [N], C_d, v_{ij} [m/s], and S [m^2] denote the fluid drag forces acting on j-th segment of i-th link, the drag coefficient, velocities of the j-th segment of i-th link, the frontal area of the link in contact with the fluid.

The equation of motion for 2-DoF robotic arm is well-known, which is defined by:

$$\boldsymbol{M}\ddot{\boldsymbol{q}} + \boldsymbol{c}(\boldsymbol{q}, \dot{\boldsymbol{q}}) + \boldsymbol{f_d}(\dot{\boldsymbol{q}}) = \boldsymbol{\tau} \tag{3}$$

where $\boldsymbol{M}$, $\boldsymbol{q}$, $\boldsymbol{c}$, $\boldsymbol{f_d}$, and $\boldsymbol{\tau}$ denote inertia matrix, generalized coordinate ($[q_1, q_2]^{\mathrm{T}}$), centrifugal and coriolis force vector, fluid drag force vector, and joint torque ($[\tau_1, \tau_2]^{\mathrm{T}}$), respectively. The fluid drag vector $\boldsymbol{f_d}$ is described by:

$$\boldsymbol{f_d} = \begin{bmatrix} \sum_{j=1}^{N} (r_{1j} f_{d,1j} + r_{2j} f_{d,2j}) \\ \sum_{j=1}^{N} r_{2j} f_{d,2j} \end{bmatrix} \tag{4}$$

where N and r_{ij} denote the number of divisions and the lengths from the each joint to the center of the j-th segment, respectively. In reality, since the base of Lamprey-1 is not fixed, the general equations of motion for 2-DoF manipulators do not strictly apply. However, by applying this model, it is possible to calculate the required adhesion force at the base, which will be discussed next.

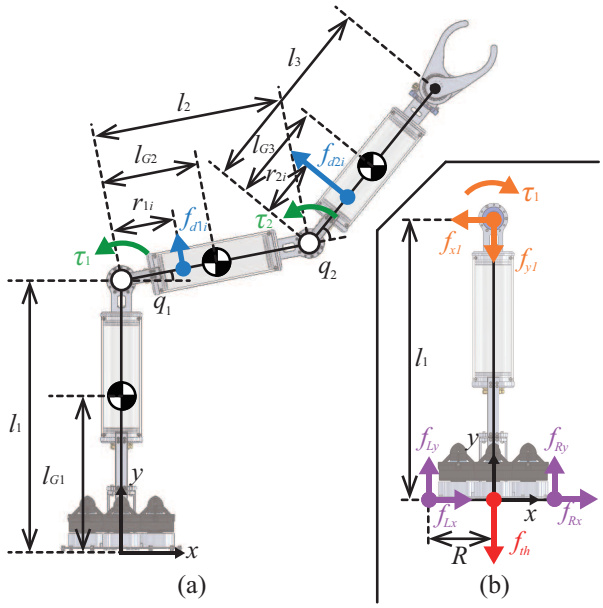

Fig. 4. Kinematic and dynamic model of the robot

B. Required suction force for wall adhesion

Figure 4 (b) shows the static model of Link 1. Link 1 receives suction force of f_{th} from thrusters, reaction forces from Link 2 (f_{x1} and f_{y1}), and reaction forces from the wall (f_{Ly} and f_{Ry}). It is assumed that the friction forces f_{Lx} and f_{Rx} are applied at the rubber bumpers of the NPEP. To simplify the model, here it was considered the forces only apply at the right and left side.

The force equilibrium along the x-axis and y-axis can be

calculated as follows:

$$f_{x1} + f_{Lx} + f_{Rx} = 0 \tag{5}$$
$$f_{Ly} + f_{Ry} + f_{y1} + f_{th} = 0 \tag{6}$$

The maximum static friction forces $f_{Lx,\max}$ and $f_{Rx,\max}$ are given by

$$f_{Lx,\max} = \mu f_{Ly} \geq f_{Lx} \tag{7}$$
$$f_{Rx,\max} = \mu f_{Ry} \geq f_{Rx} \tag{8}$$

where μ is the coefficient of static friction.

1) Based on Eqs. (5), (7), and (8), the absolute value of the suction force required to prevent slipping on the wall $f_{th,\mathrm{slip}}$ can be calculated by:

$$f_{th,\mathrm{slip}} = -\left|\frac{f_{x1}}{\mu}\right| - f_{y1} \tag{9}$$

2) Based on eq. (6), the absolute value of the suction force required to prevent Link 1 from separating from the wall $f_{th,\mathrm{sepa}}$ can be derived by:

$$f_{th,\mathrm{sepa}} = -f_{y1} \tag{10}$$

3) The absolute value of the suction force required to prevent the NPEP from separating by tilting around its endpoint $f_{th,\mathrm{tilt}}$ can be calculated by:

$$f_{th,\mathrm{tilt}} = \begin{cases} \frac{l_1}{R} f_{x1} - f_{y1} - \frac{\tau_1}{R} & (\tau_1 - l_1 f_{x1} \geq 0) \\ -\frac{l_1}{R} f_{x1} - f_{y1} + \frac{\tau_1}{R} & (\tau_1 - l_1 f_{x1} < 0) \end{cases} \tag{11}$$

where R is the distance between the center of the NPEP and the contact point

The minimum suction force to prevent Link 1 from separating from the wall is defined as the maximum absolute value among $f_{th,\mathrm{slip}}$, $f_{th,\mathrm{sepa}}$, and $f_{th,\mathrm{tilt}}$ based on Eqs. (9), (10), and (11).

IV. EXPERIMENTS

A. The relationship between ESC input value and the suction force

The suction force of the thruster is generally unknown, thus, the relationship between the ESC input value to each thruster and the suction force was experimentally predetermined. The experimental procedure is as follows. The Link 1 separated to other links was connected to a force gauge (ZTS-500N; IMADA Inc., Aichi, Japan) with a wire. Then, the NPEP bumpers were contacted with the pool bottom, and the force gauge was slowly pulled vertically upwards after the thrusters have completed their full rotation. Five different PWM (pulse width modulation) duty ratios, 7.75%, 7.875%, 8%, 8.125%, and 8.25%, were provided to the ESC input. Measurements were performed at least five times for each input pattern. The average of the maximum force values in each measurement and subtracting the underwater gravity value of Link 1 from this was defined as the suction force. It was revealed that when the ESC input value was less than 7.75% of the PWM duty ratio, the thrusters did not rotate at all, while when it was more than 8.25%, the power supply

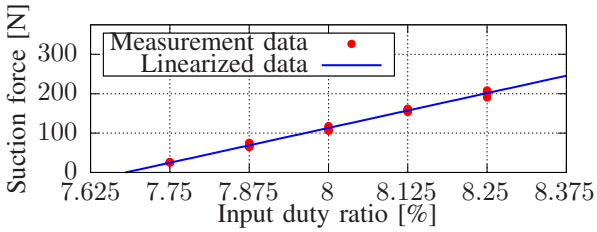

Fig. 5. Relationship between the PWM duty ratio for the thruster and the actual suction force measured from the preliminary test

TABLE I
PARAMETER COMBINATIONS FOR DIFFERENT ARM-END TRAJECTORIES

Num	A_x	ω_x	B_x	C_x	A_y	ω_y	B_y	C_y
1	0	0	0	0.55	0.3	0.8	0	0.7
2	0	0	0	0.55	0.3	1.3	0	0.7
3	0	0	0	0.8	0.3	0.8	0	0.7
4	0	0	0	0.8	0.3	1.3	0	0.7
5	0.5	0.3	0	0	0	0	0	1.1
6	0.5	0.5	0	0	0	0	0	1.1
7	0.5	0.3	0	0	0	0	0	1.3
8	0.5	0.5	0	0	0	0	0	1.3
9	0.15	0.8	0	0	0.15	0.8	$-\pi/2$	1.25
10	0.15	1.3	0	0	0.15	1.3	$-\pi/2$	1.25
11	0.15	-0.8	0	0	0.15	-0.8	$-\pi/2$	1.25
12	0.15	-1.3	0	0	0.15	-1.3	$-\pi/2$	1.25

falls into a power shortage. Therefore, we decided to use the PWM duty ratio within this range.

Figure 5 shows a linear approximation of the relationship between each ESC input value and the measured suction force. This linear interpolation yielded the following equation:

$$f_{\mathrm{est}} = 353.65 u_{\mathrm{in}} - 2716.1 \tag{12}$$

where f_{est} is the estimated suction force, and u_{in} is ESC input value. This experiment showed that Lamprey-1 can generate a maximum suction force of 200 N.

B. Suction experiments with different arm trajectories in simulation and real

Here, experiments were conducted both in simulation and with actual robot to investigate whether Lamprey-1 can maintain the wall suction while its arm is operating. The target arm-end positions x_d and y_d were given by:

$$x_d = A_x cos(\omega_x t + B_x) + C_x \tag{13}$$
$$y_d = A_y cos(\omega_y t + B_y) + C_y \tag{14}$$

where A_x and A_y are the amplitudes, ω_x and ω_y are the angular frequencies, B_x and B_y are the phase differences, and C_x and C_y are the oscillation centers.

Table I lists the parameter combinations for the target trajectories. The trajectory num. 1-4, 5-8, and 9-12 correspond to horizontal, vertical, circular movements of the arm-end, respectively.

1) Experiments in simulation: Table II lists the used for the simulation. In this simulation, the twelve target end-effector trajectories were input into the inverse kinematics model of a general planar 2-DoF robotic arm and converted

TABLE II

PARAMETERS USED FOR THE SIMULATION

Link 2 and weight mass	m_2	2.92 kg
Link 3 and the end-effector mass	m_3	3.93 kg
Moment of inertia of link 2	I_2	0.326 kgm^2
Moment of inertia of link 3	I_3	0.840 kgm^2
Link length 1	l_1	0.538 m
Link length 2	l_2	0.4745 m
Link length 3	l_3	0.4545 m
Link diameter	D	0.108 m
Distance to CoM of link 2	l_{G2}	0.2975 m
Distance to CoM of link 3	l_{G3}	0.2430 m
Drag coefficient of link 2	C_{d2}	0.9
Drag coefficient of link 3	C_{d3}	1.2
Added-mass coefficient of link 2	C_{m2}	4.3
Added-mass coefficient of link 3	C_{m3}	4.5
Water density	ρ	1000 kg/m^3
Disk-center-to-contact-point distance	R	0.14 m
Friction coefficient	μ	0.14
Number of divisions	N	100
Sampling time	dt	0.01 ms

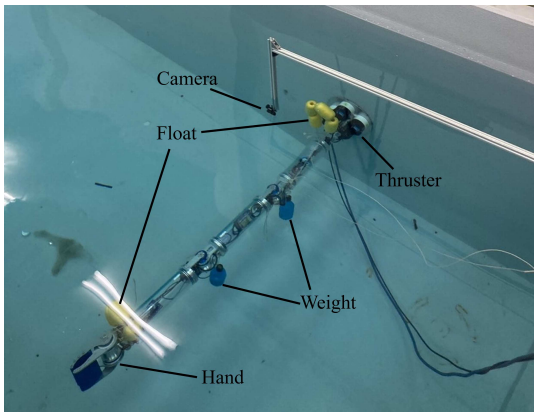

Fig. 6. Experimental setup to verify the behavior during the underwater wall suction with different arm trajectories

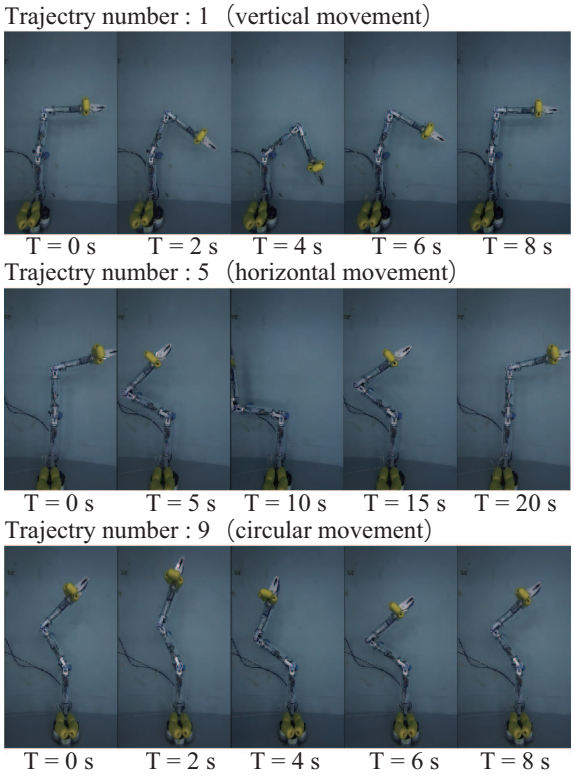

Fig. 7. Motion transitions of Lamprey-1 during three different trajectories; 1 (horizontal), 5 (vertical), and 9 (circular) with PWM duty ratio of 8%

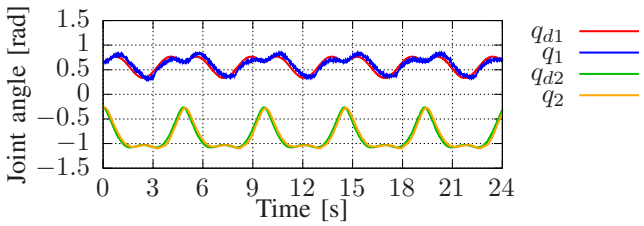

Fig. 8. Target and measured angles of each joint in trajectry number 4

into joint angles. Subsequently, the joint torques, which serve as control inputs, were calculated from the PD control law of these target joint angles and fed into the robot's dynamics model described by Eq. (3). Finally, the adhesive force required to keep the robot from detaching from the wall was calculated using Eqs. (9), (10), and (11) from the internal force acting on the joints between Links 1 and 2 (f_{x1} and f_{y1}), as computed in this process.

2) Experiments with actual robot: Figure 6 shows the overview of the experimental setup. Figure 7 shows the motion transitions of Lamprey-1 during three different trajectories; 1 (horizontal), 5 (vertical), and 9 (circular). As an example, the target angle of each joint (q_{d1}, q_{d2}) and their corresponding measured joint angle in the target arm-end trajectory 4 were plot in Fig. 8. This result indicates that the joint is tracking the target value. The suction force in the experiment was estimated from Eq. (12).

C. Verification of the results

Table III lists the results of the adhesion feasibility in both simulation and actual experiment. ✓ denotes that suction was succeeded, whereas "F" denotes failed. The comparison results between this simulation and the actual robot experiment revealed that, except for trajectory num. 5 and 7 at an adhesive force of 24.8 N, the feasibility of adhesion could be estimated for all combinations.

This is because the deviation between the fluid drag model and the actual phenomenon increases with end-effector speed. The added-mass coefficient used in our model is much larger than the typical value ($C_{m2} = C_{m3} = 1$) since the fluid drag of the end-effector was not considered in this simulation.

In this comparison, due to the constraints of selecting PWM duty ratios, only three adhesion force patterns were prepared. Therefore, it is expected that increasing the adhesion force resolution for comparison would allow for a finer identification of the adhesion feasibility boundary. This could potentially be achieved, for example, by finely adjusting the adhesion force of each of the four thrusters individually.

In addition, in all of the failure, the robot rotated around the NPEP endpoint and separated from the wall. This result

TABLE III

COMPARISON RESULTS OF WALL ADHESION CAPABILITY IN SIMULATION AND ACTUAL EXPERIMENT ("F" MEANS FAILD)

Suction force	**-24.8 N**		**-69.0 N**		**-113.1 N**	
Num	Sim.	Act.	Sim.	Act.	Sim.	Act.
1	F	F	✓	✓	✓	✓
2	F	F	F	F	✓	✓
3	F	F	✓	✓	✓	✓
4	F	F	F	F	✓	✓
5	✓	F	✓	✓	✓	✓
6	F	F	✓	✓	✓	✓
7	✓	F	✓	✓	✓	✓
8	F	F	✓	✓	✓	✓
9	✓	✓	✓	✓	✓	✓
10	F	F	✓	✓	✓	✓
11	✓	✓	✓	✓	✓	✓
12	F	F	✓	✓	✓	✓

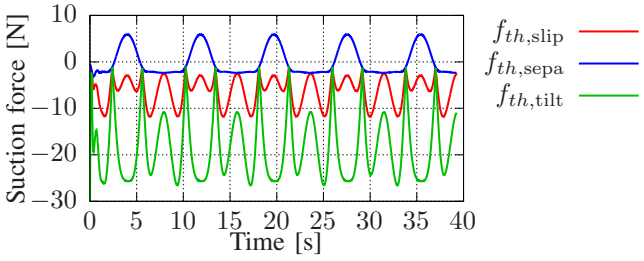

Fig. 9. Adhesive forces required for wall suction in trajectry number 1

is also supported by our simulations. As plot in Fig. 9, among three adhesive forces required for wall adsorption in the simulation ($f_{th,\mathrm{slip}}$, $f_{th,\mathrm{sepa}}$, and $f_{th,\mathrm{tilt}}$), $f_{th,\mathrm{tilt}}$ is the smallest (the absolute value of the required adsorption force is the largest). This means that when gradually decreasing the adsorption force from the complete adsorbed state, the NPEP first peels off while rotating around the endpoint. In other words, unless the thrusters are suddenly shut off, there will be no sudden slipping or the NPEP completely detaching from the wall. Fig. 9 only shows the results in trajectry number 1, however, the results were identical for other trajectories.

V. CONCLUSIONS

In this paper, the first prototype of an articulated-arm underwater robot with thrusters for both suction and propulsion named Lamprey-1 was proposed. This study focused on the adhesion force required when Lamprey-1 moved its arm-end along three different trajectories. The validity of this derivation was verified not only through simulation but also through underwater experiments using the actual robot.

The results revealed that for 10 out of 12 trajectories, the robot's wall adhesion feasibility could be determined through pre-calculation. Notably, these results were obtained by tuning the added inertia coefficient and fluid drag coefficient, despite the model being very simple and ignoring the actual hand component. For the remaining two trajectories, when the adhesive force increased, the simulation results matched the actual robot experiment results. Since the resolution of the adhesive force options is not particularly high, to make the adhesion feasibility determination more accurate, it is necessary to perform fine-grained adhesive force adjustments.

In the future, it will be also necessary to design not only the entire robot for neutral buoyancy but also each individual link for neutral buoyancy to prevent the whole posture rotation during the robot motion. This will eliminate the need for unnecessary floats or weights, as used in the current experiments. Furthermore, beyond the adhesion feasibility determination described in this paper, it is also necessary to verify methods for dynamically varying the adhesion force according to the position and speed of the arm's end effector. This will enable the thrusters' energy consumption to be minimized, increasing the potential for longer-duration adhesion.

REFERENCES

[1] P. Ridao, M. Carreras, D. Ribas, P. J. Sanz, and G. Oliver, "Intervention AUVs: The Next Challenge," in *Proc. 19th World Congress, IFAC*, pp. 12146-12159, 2014.

[2] E. Simetti, G. Casalino, S. Torelli, A. Sperindé, and A. Turetta, "Floating Underwater Manipulation: Developed Control Methodology and Experimental Validation within the TRIDENT Project," *J. Field Robotics*, vol. 31, no. 3, pp. 364-385, 2014.

[3] E. Simetti, F. Wanderlingh, S. Torelli, M. Bibuli, A. Odetti, G. Bruzzone, D. L. Rizzini, J. Aleotti, G. Palli, L. Moriello, and U. Scarcia, "Autonomous Underwater Intervention: Experimental Results of the MARIS Project," *IEEE J. Ocean. Eng.*, vol. 43, no. 3, pp. 620-639, 2018.

[4] J. E. Manley, S. Halpin, N. Radford, and M. Ondler, "Aquanaut: A New Tool for Subsea Inspection and Intervention," in *Proc. OCEANS 2018 MTS/IEEE Charleston*, pp. 1-4, 2018.

[5] A. Birk, T. Doernbach, C. A. Müller, T. Luczynski, A. G. Chavez, D. Köhntopp, A. Kupcsik, S. Calinon, A. K. Tanwani, G. Antonelli, P. di Lillo, E. Simetti, G. Casalino, G. Indiveri, L. Ostuni, A. Turetta, A. Caffaz, P. Weiss, T. Gobert, B. Chemisky, J. Gancet, T. Siedel, S. Govindaraj, X. Martinez, and P. Letier, "Dexterous Underwater Manipulation from Onshore Locations: Streamlining Efficiencies for Remotely Operated Underwater Vehicles," *IEEE Robot. Autom. Mag.*, vol. 25, no. 4, pp. 24-33, 2018.

[6] P. Liljebäck and R. Mills, "Eelume: A Flexible and Subsea Resident IMR Vehicle," in *Proc. OCEANS 2017 - Aberdeen*, pp. 1-4, 2017.

[7] R. Pi, P. Cieślak, J. Esteba, N. Palomeras, and P. Ridao, "Compliant Manipulation With Quasi-Rigid Docking for Underwater Structure Inspection," *IEEE Access*, vol. 11, pp. 128957-128969, 2023.

[8] N. Sakagami, K. Ishimaru, S. Kawamura, M. Shibata, H. Onishi, and S. Murakami, "Development of an Underwater Robotic Inspection System Using Mechanical Contact," *J. Field Robotics*, vol. 30, no. 4, pp. 624-640, 2013.

[9] A. A. F. Nassiraei, T. Sonoda, and K. Ishii, "Development of Ship Hull Cleaning Underwater Robot," in *Proc. 5th Int. Conf. Emerging Trends Eng. Technol.*, pp. 157-162, 2012.

[10] N. Sakagami, Y. Yumoto, T. Takebayashi, and S. Kawamura, "Development of Dam Inspection Robot With Negative Pressure Effect Plate," *J. Field Robotics*, vol. 36, no. 8, pp. 1422-1435, 2019.

[11] T. Iwahori, T. Takebayashi, N. Sakagami, and S. Kawamura, "Computational and Experimental Investigation of a Negative Pressure Effect Plate for Underwater Inspection Robots," in *Proc. IEEE/SICE Int. Symp. System Integration (SII)*, pp. 239-243, 2021.

[12] N. Sakagami, M. Fukami, Y. Tanaka, A. Koshioka, and A. Kakogawa, "Testing a Portable Underwater Robotic Manipulator with a Structure-Wall Suction Mechanism," in *Proc. AROB 30th 2025 / ISBC10 / SWARM8*, pp. 681-684, 2025.

[13] A. Kakogawa, S. D. Rajendrakumar, and Y. Iwasaki, "Grasping of Cylindrical Structures Using an Underwater Snake Robot Without Force/Torque Sensors and Actuator Waterproofing," *J. Robotics Mechatronics*, vol. 36, no. 6, pp. 1458-1467, 2024.

[14] T. Shimooka, A. Kakogawa, and H. Tanaka, "An Agile Robotic Penguin Driven by Submersible Geared Servomotors: Various Maneuvers by Active Feathering of the Wings," in *Proc. IEEE/RSJ Int. Conf. Intell. Robots Syst. (IROS)*, pp. 303-308, 2024.